

Shoaling of abyssal ventilation in the Eastern Indian Sector of the Southern Ocean

Keishi Shimada ^{1✉}, Yujiro Kitade², Shigeru Aoki ³, Kohei Mizobata ², Lingqiao Cheng ^{4,5}, Kunio T. Takahashi^{6,7}, Ryosuke Makabe^{2,6,7}, Jota Kanda ^{2,6} & Tsuneo Odate^{6,7,8}

Antarctic Bottom Water formation, which ventilates the abyssal layers of the Southern Ocean, is an integral component of the global ocean meridional overturning circulation. Considering evident freshening and density decreases in the source waters, widespread warming in the Southern Ocean suggests a weakening in the Antarctic Bottom Water supply. We demonstrate that the weakening is robust based on water mass warming in the deep and abyssal layers of the Australian-Antarctic Basin, which remained after removing the southward shift effect of the Southern Antarctic Circumpolar Current Front. Moreover, a decrease in apparent oxygen utilisation and reduced warming in the intermediate density layer below Circumpolar Deep Water extended further from the Australian-Antarctic Basin to the South Australian Basin. We suggest that a concurrent weakening in the densest portion and strengthening in the less dense portion shape the multi-basin change in the meridional overturning circulation that originates from the Southern Ocean.

¹Centre for Marine Research and Operations, Tokyo University of Marine Science and Technology, 4-5-7, Kounan, Minato-ku, Tokyo 108-8477, Japan.

²Department of Ocean Sciences, Tokyo University of Marine Science and Technology, 4-5-7, Kounan, Minato-ku, Tokyo 108-8477, Japan. ³Institute of Low Temperature Science, Hokkaido University, Kita-19, Nishi-8, Kita-ku, Sapporo 060-0819, Japan. ⁴College of Marine Sciences, Shanghai Ocean University, No. 999, Huchenghuan Rd., Lingang Special Area, Shanghai 201306, China. ⁵Centre for Polar Research, Shanghai Ocean University, No. 999, Huchenghuan Rd., Lingang Special Area, Shanghai 201306, China. ⁶National Institute of Polar Research, Research Organization of Information and Systems, 10-3 Midori-cho, Tachikawa, Tokyo 190-8518, Japan. ⁷Department of Polar Science, The Graduate University for Advanced Studies (SOKENDAI), 10-3 Midori-cho, Tachikawa, Tokyo 190-8518, Japan. ⁸Deceased: Tsuneo Odate. ✉email: kshima0@kaiyodai.ac.jp

The deep and abyssal layers of the Southern Ocean are undergoing evident warming and freshening, thereby considerably contributing to global heat and freshwater budgets^{1,2}. Antarctic Bottom Water (AABW), which is an integral component of the global ocean meridional overturning circulation (MOC), forms in the Southern Ocean owing to high sea ice production and strong cooling in the coastal regions³. AABW accounts for 30–40% of the global ocean water mass⁴. Hence, clarifying the characteristics and drivers of change in AABW is critical for improving our understanding of future climatic conditions. Sea level rise (SLR) in the high latitude region south of 62° S exceeds the global mean by 1–5 (mm year⁻¹)⁵, and SLR in the Australian-Antarctic Basin (AAB) is the highest at basin scale among the major basins adjacent to Antarctica (Fig. 1b). Along with magnitude, these spatial variations are also critical because they may reflect source and path of accelerated freshwater supply from the Antarctic Ice Sheet and also variation in formation and circulation of AABW⁵.

One of the major causes of the warming is considered to be a weakened AABW supply (here, the weakened supply includes both reduction in the AABW formation rate with relatively constant temperature^{1,6–8}, and warming in the formed AABW with a relatively constant formation rate^{8,9}). Because warming in the dense shelf water (DSW), which is the source water of AABW, is weak⁸, rapid freshening of DSW^{10–12} is the likely cause for the weakened AABW supply. In other words, rapid freshening reduced the potential energy required for DSW to sink into the abyss. Another potential cause of the warming is the southward shift in the Antarctic Circumpolar Current (ACC) fronts, which also induce southward shift in warm water masses locate in the north¹³, although the robustness of this phenomenon and its overall effect on the Southern Ocean remain under debate¹⁴. Therefore, the current condition of the change in the AABW

supply and its impact on the MOC and the global climate are not clear.

The training and research vessel *Umitaka-Maru* of Tokyo University of Marine Science and Technology conducted observations beginning in 2011 to obtain high-quality top-to-bottom summer hydrographic data on the offshore region between the Vincennes Bay and Sabrina coast (East Antarctica, Fig. 1a). By combining data obtained at the World Ocean Circulation Experiment (WOCE) Hydrographic Programme or the Global Ocean Ship-Based Hydrographic Investigation Program (GO-SHIP) I09s section, long-term abyssal warming, freshening, and density decrease after the 1990s can be confirmed in both the South Australian Basin (SAB) and AAB (Fig. 1a insets). The region covering the data points in the southern region of the AAB is referred to as the core region in the AAB (core AAB), corresponding to the area encompassed by solid lines shown in Fig. 1a; Supplementary Note S1 provides a detailed description of the hydrographic data.

In this study, we demonstrate that evident warming signals remain robust in the deep and abyssal layers of the AAB, even after removing the effect of the southward shift in the Southern ACC Front (SACCF; Fig. 1), which is estimated as 55 ± 30 km during observed period spanning 25 years. This fact suggests that AABW supply has weakened. We further show that the ventilating layers shifted toward less dense and shallower layers. Rapid and persistent freshening in DSW reduced its density, and a part of less dense DSW flowed down to shallower layers instead of sinking down to abyssal layers. Therefore, the structure of the lower limb of the MOC (LMOC) in the AAB and SAB has changed such that the densest portion in the abyssal layers has weakened and the relatively less dense portion has intensified in the mid to deep layers.

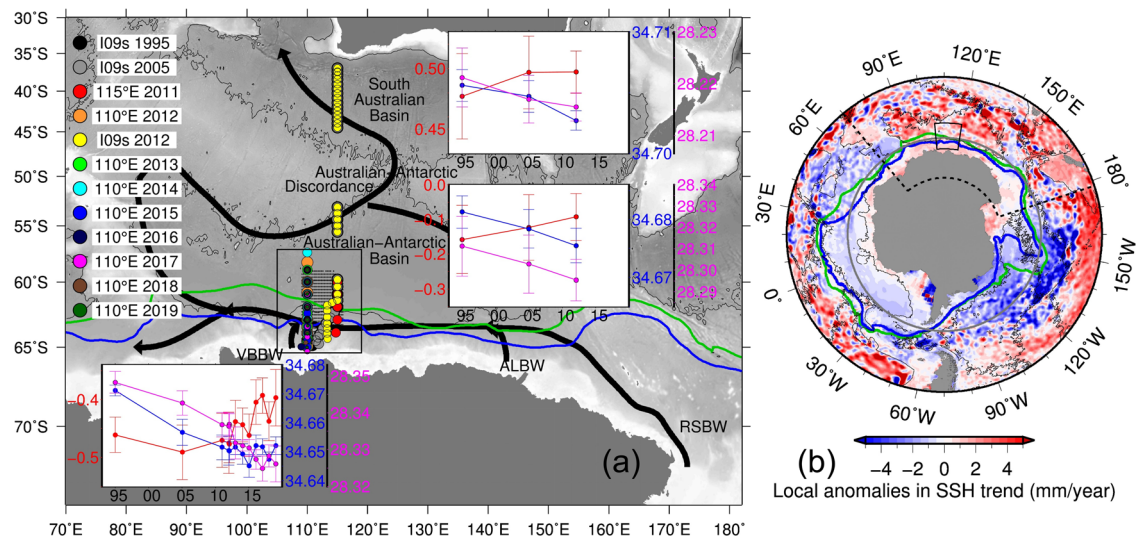


Fig. 1 Location of the study area with a schematised Antarctic Bottom Water (AABW) pathway and satellite-observed sea-level rise (SLR) in the Southern Ocean. **a** Observation points are coloured according to year. The solid black frame indicates the core region in the Australian-Antarctic Basin (core AAB). The hatched area indicates satellite altimeter data points used for comparison with steric SLR. Black arrows indicate AABW pathways³³; major sources of Ross Sea Bottom Water¹⁵, Adélie Land Bottom Water¹⁹ and Vincennes Bay Bottom Water²² are shown. The solid black line indicates the 4000 m isobath. Upper, middle and lower insets are the time series of the bottom properties in the South Australian Basin, northern AAB and core AAB, respectively. In each inset, potential temperature (red), practical salinity (blue), and neutral density (pink) averaged over 100 m from bottom are shown with error bar indicating standard deviation. **b** Local anomalies in sea-surface height (SSH) trends compared to the overall Southern Ocean. Linear SSH trends were estimated at each data point, and the mean rate of SLR in the Southern Ocean was subtracted. Only satellite altimeter data from ice-free months (January–April) between 1993 and 2018 were used⁵. The solid black and grey lines in **b** indicates the 4000 m isobath and 62°S latitude, respectively. The areas encompassed by broken and solid lines correspond to the entire domain of **a** and the core AAB region, respectively. The green and blue lines in **a** and **b**, respectively, indicate climatological position of the Southern Antarctic Circumpolar Current Front and southern boundary³⁴ estimated using observed data prior to the year 2013³².

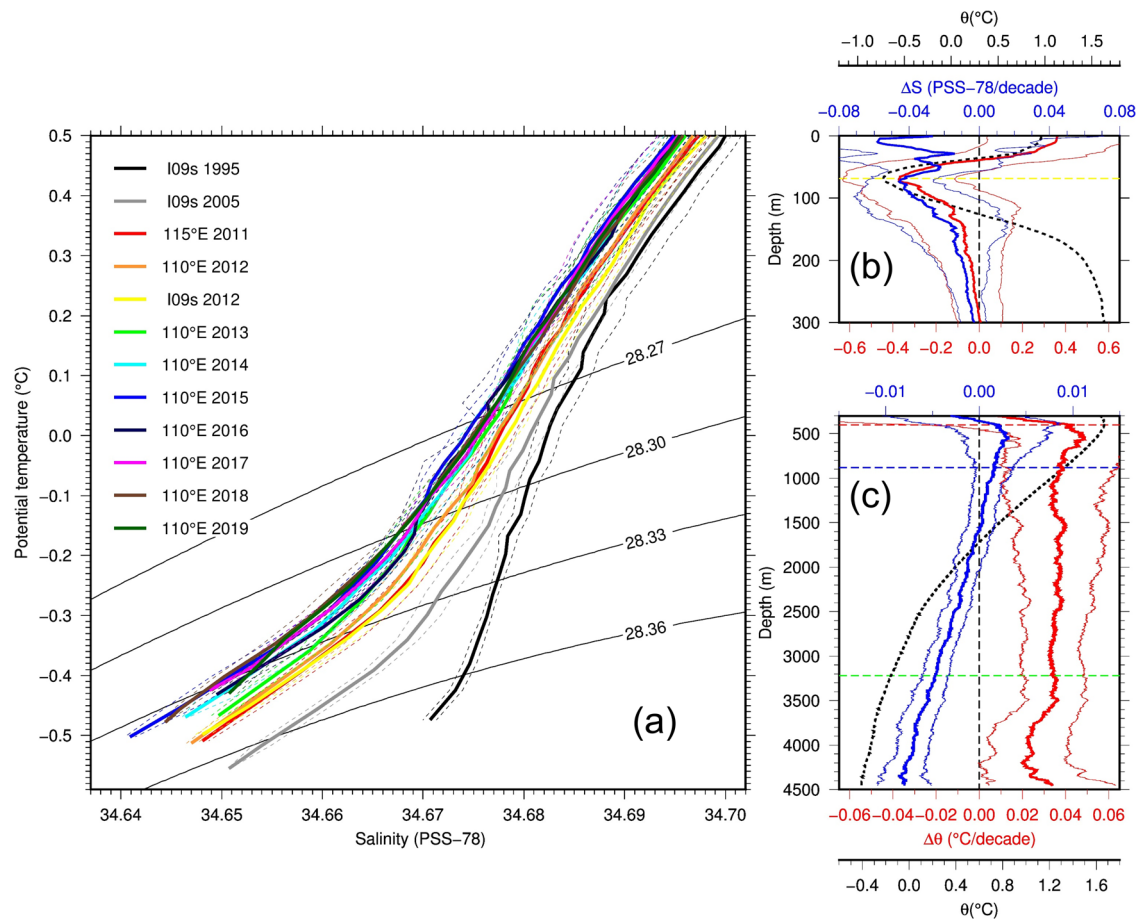


Fig. 2 Multi-decadal variability in potential temperature and salinity in the core region in the Australian-Antarctic Basin (core AAB). **a** θ - S changes in the core AAB. θ - S curves were averaged on isopycnal surfaces for each section, and broken lines indicate standard deviations. θ - S curves are coloured according to the observation year in the same manner as the observation points in Fig. 1a. **b**, **c** are vertical profiles of the linear trends in potential temperature (red) and salinity (blue) in layers above and below 300 m, respectively. Thin lines indicate the 95% confidence interval. Note that the abscissa is substantially different. The profile of the mean (spatio-temporal) potential temperature is shown by the black broken lines. The depth of the potential temperature minimum, potential temperature maximum, salinity maximum and $\gamma^n = 28.30 \text{ kg m}^{-3}$ (corresponding to the top layer of the Antarctic Bottom Water) are shown by yellow, red, blue and green broken lines, respectively.

Results and discussion

Long-term warming and freshening throughout the water column and extensive SLR in the AAB. The θ - S curves in the deep layer below the 0.5°C isotherm ($\sim 1900 \text{ m}$) exhibited bottom-intensified and widespread freshening throughout the study period, although it became moderate after 2015 (Fig. 2a). Deep layer freshening below the 0°C isotherm ($\sim 2800 \text{ m}$) in 2005 (Fig. 2a) was spread up to the 0.7°C isotherm ($\sim 1600 \text{ m}$), although the statistical significance becomes marginal above the 0.35°C isotherm ($\sim 100 \text{ m}$; Fig. 2c). These results indicate that freshening has spread to $\sim 80\%$ of the layers below the salinity maximum layer ($\sim 900 \text{ m}$), which correspond to lower circumpolar deep water¹⁵. Multi-decadal AABW freshening was determined by averaging the linear trends of layers below the climatological isopycnal of $\gamma^n = 28.3 \text{ kg m}^{-3}$ ($\sim 3226 \text{ m}$), where we identified significant freshening at a rate of $-0.0064 \pm 0.0020 \text{ decade}^{-1}$. The estimated rate was consistent with that estimated in upstream region of the AABW pathway at WOCE/GO-SHIP section SR3 located at 140° E ($-0.0083 \pm 0.0023 \text{ decade}^{-1}$)¹⁶, as well as with that estimated using the most recent observations in downstream region at I08s located from 82 to 95° E ($-0.0080 \pm 0.0010 \text{ decade}^{-1}$)¹⁷. Warming exhibited a further vertical extent, which was significant below the temperature maximum layer ($\sim 400 \text{ m}$ or 1.7°C isotherm; Fig. 2c), greatest in

the mid to deep layers (500 – $3,500 \text{ m}$), and slightly reduced towards the bottom. The AABW warming rate ($0.028 \pm 0.018 \text{ }^\circ\text{C decade}^{-1}$) was consistent with the estimations obtained in downstream region at I08s ($0.020 \pm 0.030 \text{ }^\circ\text{C decade}^{-1}$ from 1994 to 2007 and $0.060 \pm 0.010 \text{ }^\circ\text{C decade}^{-1}$ from 2007 to 2016)¹⁷.

Widespread warming and freshening in both the shallow and deep layers influenced the sea level (Fig. 3 and Table 1). Over the study period, the steric SLR (density-induced; grey circles and line) and SLR derived from the satellite altimeter data (satellite SLR; dark green circles) increased with time. While the satellite SLR trend ($3.2 \pm 1.3 \text{ mm decade}^{-1}$) was larger than that of the steric SLR ($2.7 \pm 1.6 \text{ mm decade}^{-1}$) throughout the period, their correlation coefficient was high (up to 0.91); differences could likely be attributed to baristatic (mass-induced) SLR ($<1.5 \text{ mm y}^{-1}$)⁵, which were not included in the steric SLR estimation. The agreement indicates that our observations and analyses can effectively represent the variability in the study area.

The obtained steric SLR was then divided into four components concerning the depth (layers deeper or shallower than 2000 m) and cause (thermo/halosteric). The standard deviations of the four components were comparable (roughly within a factor of two), implying that both the thermo- and halosteric components influenced the SLR throughout the water column. Furthermore, the contribution of shallow- ($1.2 \pm 1.1 \text{ mm}$

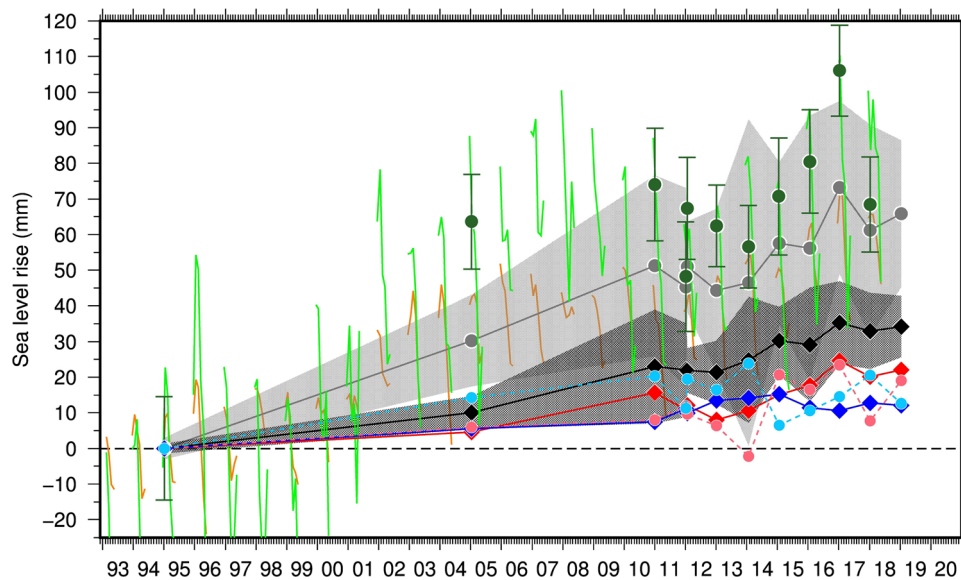


Fig. 3 Time-series of Sea Level Rise (SLR) estimated from the satellite altimeter and conductivity-temperature-depth (CTD) observations in the core region in the Australian-Antarctic Basin (core AAB). Time-series of SLR estimated from the satellite altimeter and CTD observations in the core AAB. Light green lines denote smoothed (30-d moving average) summer (January to March) satellite-observed SLR in the core AAB, and orange lines denote those of the overall Southern Ocean. Dark green circles with error bars denote 10-d means and standard deviations of the satellite-observed SLR in the core AAB over the study period, where the midpoint corresponds to the CTD observations. Grey circles and black diamonds with solid lines denote steric SLR for the entire water column and deep layers below 2000 m, respectively; the shaded area indicates the 95% confidence interval. Red and blue diamonds with solid lines denote deep layer thermo- and halosteric SLR, respectively. Pink and light blue circles with dashed lines denote thermo- and halosteric SLR in the shallow layer above 2000 m, respectively. Two points are plotted for 2012 to reflect observations along 110°E and the I09s.

Table 1 Steric and satellite-observed SLR in the study area.

	Thermosteric SLR	Halosteric SLR	Steric SLR	Satellite SLR
Water column	1.7 ± 0.9 (62 ± 33%)	1.0 ± 0.7 (38 ± 27%)	2.7 ± 1.6	3.2 ± 1.3
Shallow layers (< 2,000 m)	0.7 ± 0.6 (27 ± 21%)	0.5 ± 0.5 (18 ± 19%)	1.2 ± 1.1 (45 ± 40%)	-
Deep layers (> 2,000 m)	0.9 ± 0.3 (35 ± 12%)	0.5 ± 0.2 (20 ± 8%)	1.5 ± 0.5 (55 ± 19%)	-

Thermo- and halosteric SLR are listed separately for the deep and shallow layers (below and above 2000 m, respectively). Error indicates the 95% confidence interval, and the values in parentheses indicate the contribution to the total present steric SLR. The rate of SLR is given in mm y^{-1} .

y^{-1}) and deep-layer ($1.5 \pm 0.5 \text{ mm y}^{-1}$) components were comparable within error. The ratios of the thermo- and halosteric contributions were also comparable in the shallow and deep layers at $\sim 6:4$. However, inter-annual fluctuations were more evident in the shallow layers than in the deep layers (Fig. 3). Thus, the statistical significance of both the thermo- and halosteric components was greater in the deep layers (Table 1), where deep-layer components contributed substantially to the multi-decadal trends. Overall, the SLR estimated above is consistent with those of previous studies^{1,5} (Method section provides more details on the comparison).

Robust signals of weakened AABW supply and cause of extensive SLR. The densest portion of the LMOC in the study area consists of AABW ($>28.30 \text{ kg m}^{-3}$) supply to the AAB and slightly less dense water ($\sim 28.22 \text{ kg m}^{-3}$) transport from the AAB to the SAB through the Australian-Antarctic Discordance¹⁸, which is a relatively narrow deep zone in the Southeast Indian Ridge between 120 and 128° E (Fig. 1a). The major AABW sources supplying the AAB are the Ross Sea¹⁵, Adélie/George V Land coast^{19–21}, and Vincennes Bay²². (Hereafter the densest layers in the LMOC of the study region is referred to as densest LMOC.) Rapid freshening, density decrease in DSW in the source regions^{10–12}, and widespread warming in downstream regions (core AAB, entire AAB, and SAB)^{1,6–9,13,17} suggest a weakening

of ventilation in densest LMOC. However, interpretations are not straightforward considering the warming induced by a southward shift in the ACC fronts¹³. Temperature variability in the core AAB, in fact, is highly correlated with a shift in the meridional position of the SACCF throughout the water column; hence, its effect prevails in the core AAB (Supplementary Note S3).

To understand change in AABW supply, the observed warming and freshening in the core AAB were divided into meridional shifts and water-mass change components (Fig. 4) by using methods provided in the Method section. Water mass warming was considerably lower in the mid-to-deep layer (500–2500 m), where the meridional gradient was large (Fig. S4b). In the AABW layer, however, water mass warming remained significant, as the observed warming in the AABW layer remained relatively large compared to the meridional gradient, which was considerably reduced at lower depths. Under a positive meridional gradient (Fig. S4e), freshening increased throughout the layer below the salinity maximum layer ($\sim 900 \text{ m}$).

As a result, water-mass warming and freshening trends in the layer below the salinity maximum were 31% (0.033 ± 0.018 vs. $0.010 \pm 0.022 \text{ °C decade}^{-1}$) and 138% (-0.0030 ± 0.0017 vs. $-0.0042 \pm 0.0016 \text{ decade}^{-1}$) of the observed warming and freshening, respectively. In the AABW layer, warming and freshening were 50% (0.028 ± 0.018 vs. $0.015 \pm 0.015 \text{ °C decade}^{-1}$) and 115% (from -0.0064 ± 0.0020 vs. $-0.0074 \pm 0.0016 \text{ decade}^{-1}$) of

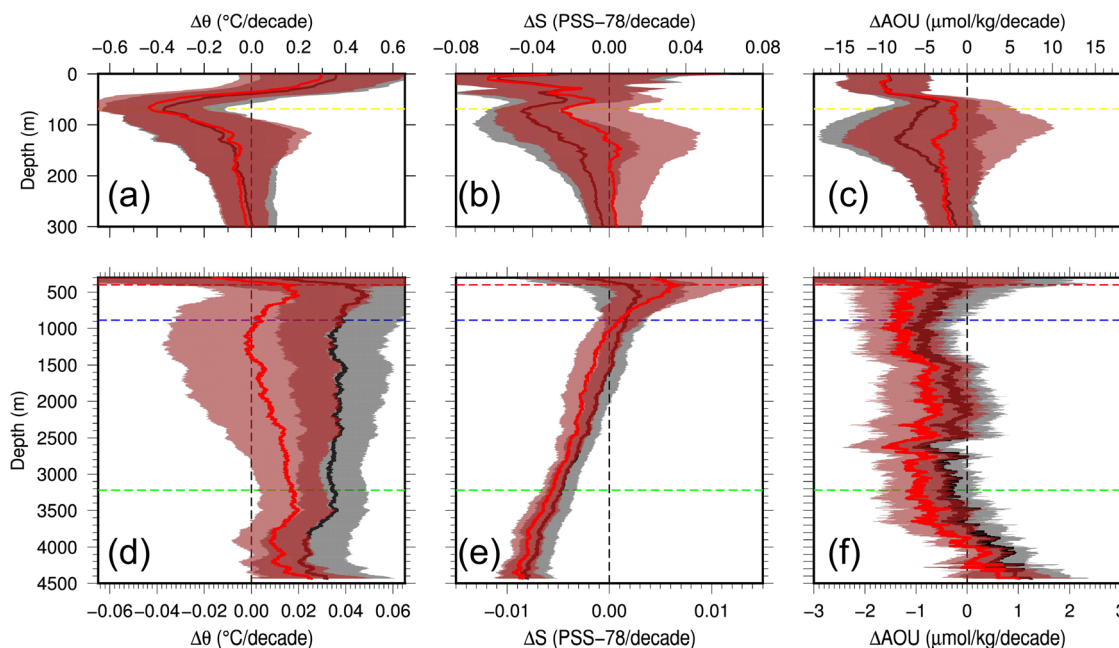


Fig. 4 Observed and water-mass change components of multi-decadal trends in the core region in the Australian-Antarctic Basin (core AAB) for the potential temperature, salinity, and apparent oxygen utilisation (AOU). The left (a, d), middle (b, e), and right (c, f) panels indicate the vertical profiles of the linear trends in potential temperature, salinity, and AOU, respectively; shallow and deep components are given in the upper (a–c) and lower (d–f) panels, respectively. In each panel, black and red lines indicate the observed and water-mass change components of the linear trends, respectively, with shaded areas indicating the 95% confidence interval. The dashed yellow, red, blue and green lines are defined in Fig. 2.

the observed warming and freshening, respectively. Hence, while the majority of the observed warming was induced by the meridional shift of the SACCF, the water-mass change component was relatively significant in the AABW layers. Furthermore, the water mass change component in apparent oxygen utilisation (AOU; a parameter which is used as a tracer for ventilation²³ and its increase/decrease indicate less/higher ventilation) revealed an increasing trend in the AABW layers (Fig. 4f). Therefore, weakening in AABW supply is evident. Based on positive meridional gradient in salinity, southward shift of the SACCF would cause salinification and hence, observed freshening is due to the water mass change component; namely, freshening in the source regions and waters. The SLR in the AAB is shown to be increased by both southward shift in the ACC and water mass change component (Supplementary Note S4). Considering the contribution of multiple factors, conditions in the AAB are favourable for an increase in SLR.

The southward shift in the ACC fronts is not evident in the SAB (Supplementary Note S5), whereas warming and AOU increase in the deep and abyssal layers below 4000 m were confirmed based on observations on the WOCE/GO-SHIP I09s (Fig. 5d, e and Supplementary Note S5). Hence, ventilation in the densest LMOC has consistently weakened.

Signals of intensified ventilation in less dense layers of LMOC.

While warming and AOU increasing prevailed in the densest LMOC, reduced or opposite signals were found in the mid to deep layer of the study area. Along the WOCE/GO-SHIP I09s section, cooling tendency and decreasing trend of AOU were found in the density range 28.02 to 28.19 kg m⁻³ (depth range of 2400 to 4200 m) of the SAB (Fig. 5d, e). Hereafter, layers with the above density range are referred to as the less dense layers of LMOC (less dense LMOC), and their upper boundary density (28.02 kg m⁻³) roughly corresponds to that of lower circumpolar deep water, which marks the vertical salinity maximum¹⁵. Similar signals are also found along the remaining WOCE/GO-SHIP

sections (I08s and SR3) in the SAB (Supplementary Note S5). In the core AAB, warming was the weakest and AOU decrease was the largest in the less dense LMOC (Fig. 5a, b). Linear trends of the entire AAB, estimated using three sections (I08s, I09s, and SR3), similarly revealed reduced warming and AOU decreasing tendency in the less dense LMOC (please note that it was difficult to remove the effect of southward shift in the ACC fronts in the case for the entire AAB; Supplementary Note S5). Hence, cooling tendency (or weak warming) and AOU decrease were widely confirmed in less dense LMOC of the study area and these signals are suggestive of intensified ventilation in these layers.

The supporting evidence for intensified ventilation was observed as increase in the intrusion of cool, fresh, and oxygen-rich water in the core AAB (Supplementary Note S6). The signals of the intrusion layers were consistent with the properties of DSW, i.e., cool, fresh, and oxygen-rich, thus these intrusions are likely derived from formation site of DSW although identification is yet difficult. The observed intrusions evidently increased after 2012, suggesting a plausible pathway for increased ventilation, although quantitative assessment is difficult owing to aliasing induced by their small spatial scale. Increases in the intrusion were further confirmed in the dense layer below the less dense LMOC (Fig. S9e–h), which likely contributed to the AOU decrease in these layers (Fig. 5b, 1700–3900 m).

The spatial structure of isopycnals and bottom topography is useful in understanding the cause of spatial structure of observed trends. The lower boundary of less dense LMOC (28.19 kg m⁻³) corresponds to the deepest isopycnal, which directly connects the AAB and SAB (Fig. 5c). The inter-basin connection at the isopycnal only occurs in the region near the Australian-Antarctic Discordance, whose depth exceeds 4000 m (Figs. 1a and 6). The connection becomes fully open for the layers above this isopycnal, thus allowing along isopycnal transport between the basins. Below the isopycnal, this transport is interrupted by the Southeast Indian Ridge and deep transport through the Australian-

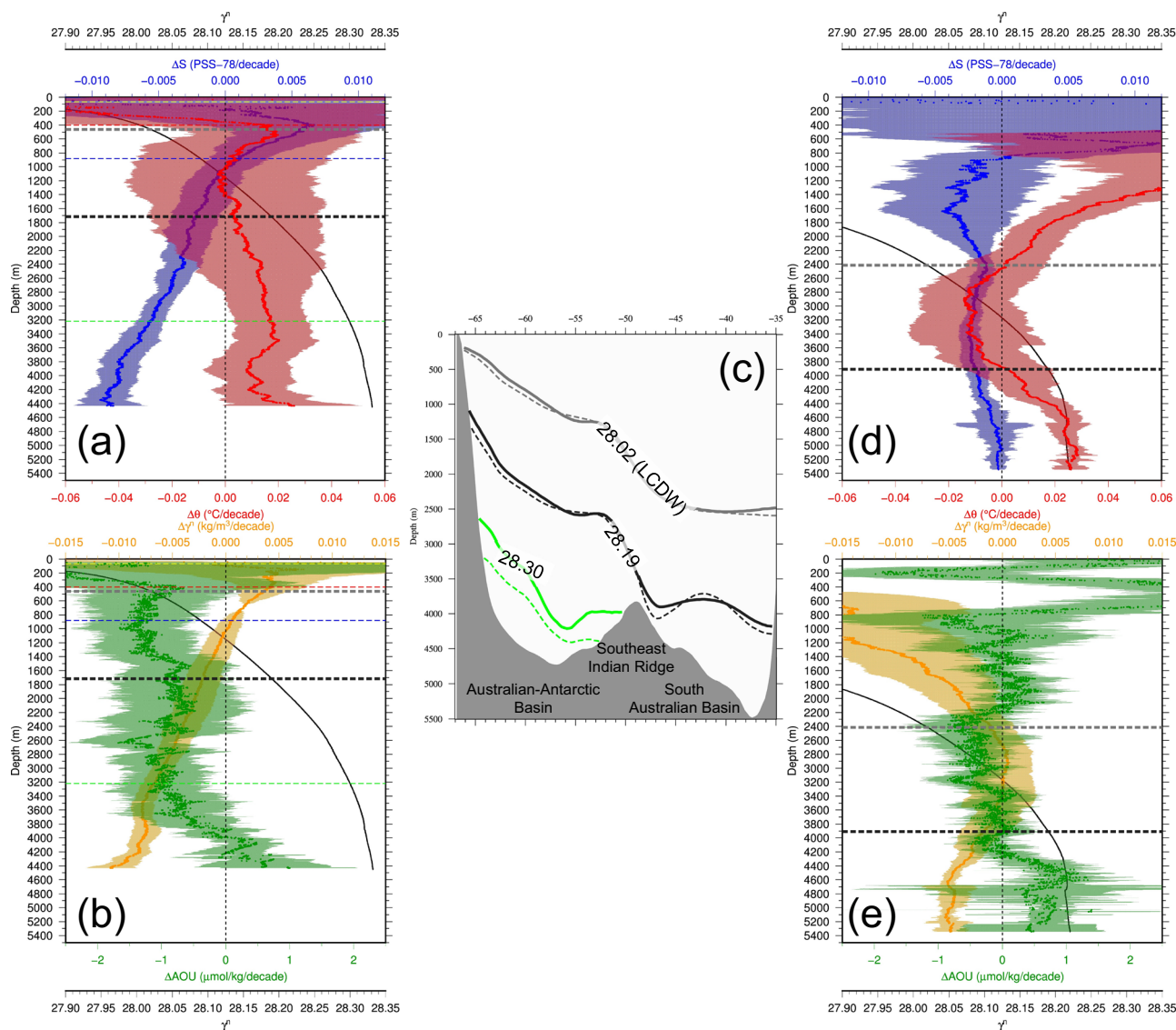


Fig. 5 Multi-decadal trends in the core region in the Australian-Antarctic Basin (core AAB) and South Australian Basin (SAB) with climatological isopycnals and bottom topography along 124° E. **a, b** are water mass change component of multi-decadal trends in the core AAB with **a** showing those of potential temperature and salinity and **b** showing those of apparent oxygen utilisation (AOU) and neutral density. **c** Labelled grey, black, and green lines indicate the isopycnals along 124°E (corresponds to middle longitude in the Australian-Antarctic Discordance) for $\sigma_t = 28.02, 28.19,$ and 28.30 kg m^{-3} , as determined by data obtained at WOCE/GO-SHIP sections SR3, I09s, and I08s, with a previously proposed interpolation scheme³². Solid lines reflect the 1994–1995 condition and broken lines reflect 2019 condition. **d, e** are observed multi-decadal trends in the SAB with **d** showing those of potential temperature and salinity and **e** showing those of AOU and neutral density. Shaded areas and black solid lines in **a, b, d** and **e** indicate 95% confidence interval and mean (spatio-temporal) neutral density, respectively. Grey and black broken lines in **a, b, d** and **e** indicate isopycnals for $\sigma_t = 28.02$ and 28.19 kg m^{-3} , respectively. The dashed yellow, red, blue, and green lines in **a, b, d** and **e** are defined in Fig. 2.

Antarctic Discordance¹⁸, which composes the densest portion of LMOC in the study area (indicated by black arrow in Fig. 1a), would contribute to cross-basinal transport.

In both the densest/less dense LMOC, AOU in the AAB is lower than the SAB along isopycnal (Supplementary Note S7) and AOU in the AAB decreased during the observed period in the layers between the upper boundary of less dense LMOC (28.02 kg m^{-3} , 450 m depth) and 3900 m depth (Fig. 5b). Based on the isopycnal distribution described above, AOU decrease in the less dense LMOC of the SAB is induced by the increased along isopycnal transport of lower AOU water and/or AOU decrease in transported water. For the layers below the less dense LMOC of the SAB, AOU increased because signals of intensified ventilation were trapped in the AAB partly owing to compensation for the reduced AABW supply (please note that depth of

lower boundary of less dense LMOC kept constant while top layer of AABW declined).

Intensification of mesoscale eddy activity^{24,25} may also decrease AOU in the SAB by increasing the exchange with the relatively oxygen-rich AAB (Supplementary Note S7). However, this is not likely because no corresponding AOU increase on both isopycnal and isobaric surfaces were observed in the AAB.

Spatial structure in salinity trends also support the intensified (weakened) ventilation in the less dense LMOC (densest LMOC). In both layers, the AAB is fresher than the SAB along isopycnal (Supplementary Note S7). Thus, even if salinity in the AAB kept constant throughout the observed period, intensification (weakening) in cross-basinal transport from AAB to the SAB will induce freshening (salinification) in both layers of the SAB. Considering that freshening in the core AAB is weak in the less dense LMOC

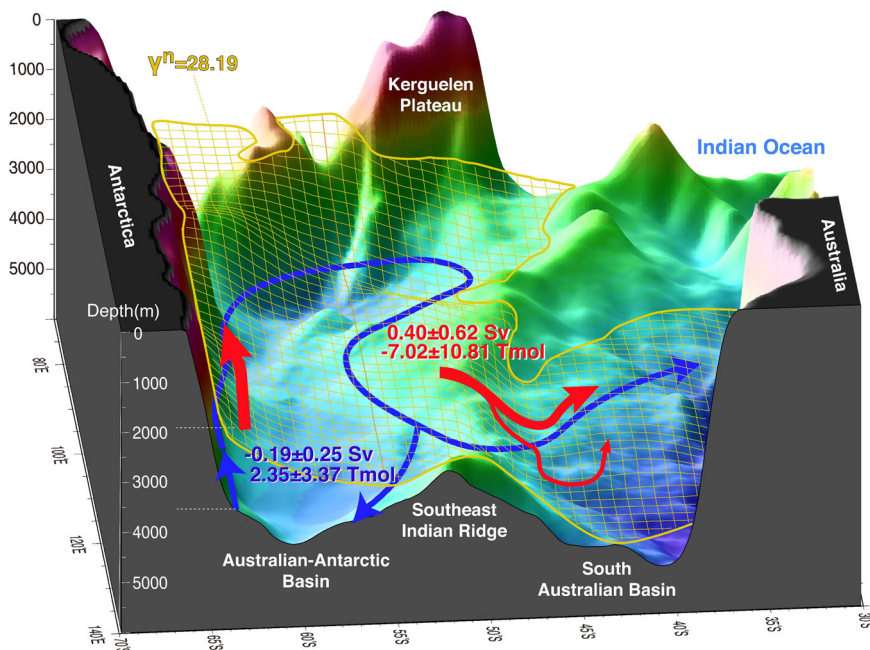


Fig. 6 Three-dimensional schematic of pathways for the densest and less dense layers of the Lower limb of the meridional overturning circulation (LMOC). The pathway in the densest layer of LMOC (densest LMOC) is shown by blue arrows and the pathways of intensified ventilation in less dense layers of LMOC (less dense LMOC) are schematised by red arrows. A meshed surface indicates a climatological isopycnal of $\gamma^n = 28.19 \text{ kg m}^{-3}$, estimated using data obtained at WOCE/GO-SHIP sections SR3, IO9s, and IO8s, with a previously proposed interpolation scheme³². The narrow pathway on less dense LMOC in the eastern South Australian Basin (SAB) reflects the fact that the observed density at the SR3 section (located from 140–147° E) is lower than the meshed isopycnals and that the apparent oxygen utilisation (AOU) decrease can be observed in the less dense layer above $\gamma^n = 28.18 \text{ kg m}^{-3}$. Total AOU changes in the densest LMOC ($\gamma^n > 28.32 \text{ kg m}^{-3}$ for the Australian Antarctic Basin and $\gamma^n > 28.19 \text{ kg m}^{-3}$ for the SAB) and less dense LMOC are shown, along with required changes in Dense Shelf Water supply.

(Fig. 5a), largest freshening in this layer of the SAB is likely induced by intensified transport of fresher water from the AAB to the SAB (similar processes is assumed for potential temperature trend). Namely, cooling tendency in SAB is induced by intensified transport of cool water from the AAB to the SAB while conclusive discussion is difficult due to large error). Considering the bottom-intensified freshening in the core-AAB (Fig. 3a), constant or intensified cross-basinal transport should induce large freshening in the deep and abyssal layers of the SAB. Thus, reduced freshening in these layers (Fig. 5d) suggests reduced cross-basinal transport.

To simply describe the magnitude of the intensified (weakened) ventilation in the less dense LMOC (densest LMOC), we estimated the total AOU changes in the respective layers by using the linear trends obtained in the core AAB and along the WOCE/GO-SHIP sections (Fig. 6). They are shown in the form of the required change in DSW supply. The AOU changes in the densest portion of the AAB ($\gamma^n > 28.32 \text{ kg m}^{-3}$) and SAB ($\gamma^n > 28.19 \text{ kg m}^{-3}$) requires a decrease in DSW supply of $-0.19 \pm 0.25 \text{ Sv}$ ($1 \text{ Sv} = 10^6 \text{ m}^3 \text{ s}^{-1}$) whereas that in the less dense LMOC requires an increase of $0.39 \pm 0.62 \text{ Sv}$. The estimated decrease in the DSW supply in the densest LMOC corresponds to a loss of the contribution from a middle-sized polynya, such as the Vincennes Bay Polynya ($0.16 \pm 0.07 \text{ Sv}$)²². Compared with the total DSW supply to the AAB, the DSW decrease in the densest LMOC corresponds to $-7 \pm 9\%$ whereas the increase in the less dense LMOC corresponds to an increase of $15 \pm 23\%$; this ratio was estimated based on the abyssal DSW supply in the overall Southern Ocean ($5.4 \pm 1.7 \text{ Sv}$)²⁶ and the sum of the contribution from the Ross Sea and Adélie/George V Land coast ($\sim 50\%$ of the total supply in the Southern Ocean)^{3,27}.

Implications of the change. We examined the intensified (weakened) ventilation in the less dense LMOC (densest LMOC). For a reduction in the net downward density flux, these changes are consistent with previous studies^{1,6–9}; however, they are clearly different on the point that shoaling occurs in the ventilating layer. Considering the widely distributed less dense LMOC over the global ocean (Supplementary Note S8), the signal of this shoaling, with a reduced topographic constraint than that for the abyssal ventilation pathway, may have been widely spread along the isopycnal. Major candidate source regions of the increased supply in the less dense LMOC are the Ross Sea and offshore region of the Adélie/George V Land coast, which are also major candidate regions of AABW source for the AAB.

Recent studies have reported a reversed signal of rapid and persistent freshening in High Salinity Shelf Water (HSSW) in the Ross Sea and AABW in the downstream region^{28–30}. How the shoaling in ventilating layer and elevated sea level would response to this reversal is a global issue. The upper boundary of the ventilation increase is currently reaching the density range of lower circumpolar deep water, which comprises the upper limit of the LMOC. Thus, if shoaling continues, further substantial changes may occur in the LMOC, followed by the changes in transport and storage of heat and other properties that influence climate, such as carbon³¹. Especially, long-term sink of anthropogenic carbon dioxide, which is an important aspect of AABW formation, is concerned to be weakened because shoaling should also occur in anthropogenic carbon transport path. Sustained observations in this region of the Southern Ocean are thus crucial for understanding ongoing and future changes in the heat and freshwater budget, SLR, MOC, and ultimately the global climate.

Methods

Determining multi-decadal trends and SLR in the core AAB. After the conditions in 1995 and observed data are gridded on each section as described in Supplementary Note S2, the multi-decadal trends and SLR in the core AAB were estimated as follows. At each vertical and horizontal grid point along the sections, changes from 1995 were calculated. Then, the time series of the changes, in the form of a vertical profile, were obtained by averaging the changes on the isobaric surfaces. Here, the averaged changes in potential temperature and salinity were expressed as $\Delta\theta_{d,i}$ and $\Delta S_{d,i}$, respectively, where d and i denote the depth coordinate and sequential number of the observations, respectively. Linear trends were obtained at each isobaric surface using the least-squares method for $\Delta\theta_{d,i}$ and $\Delta S_{d,i}$ (Fig. 2b, c).

The thermosteric and halosteric SLR were estimated separately for the shallow (<2000 m) and deep (>2000 m) layers using $\Delta\theta_{d,i}$ and $\Delta S_{d,i}$ in each section as follows:

$$\begin{aligned} \text{SLR}_{\text{thermosteric},i} &= \int \alpha \Delta\theta_{d,i} dz \text{ and} \\ \text{SLR}_{\text{halosteric},i} &= \int -\beta \Delta S_{d,i} dz, \end{aligned} \quad (1)$$

where α and β are the thermal expansion and saline contraction rates, respectively. Timeseries of estimated SLR is shown along with SLR derived from the satellite altimeter data in Fig. 3. Linear trends were estimated using the least-squares method for $\text{SLR}_{\text{thermosteric},i}$ and $\text{SLR}_{\text{halosteric},i}$ and summarised in Table 1. The estimated SLR are consistent with those of previous studies. The estimated steric SLR of $2.7 \pm 1.6 \text{ mm y}^{-1}$ is within the error of that previously estimated for the entire AAB (1.9 mm y^{-1})⁵. Deep layer thermosteric ($0.9 \pm 0.3 \text{ mm y}^{-1}$) and halosteric SLR ($0.5 \pm 0.2 \text{ mm y}^{-1}$) were comparable with those previously estimated for the entire AAB and its slope region (as shown in Fig. 6K of ref. 1), respectively.

Division of observed multi-decadal trends into frontal shift and water mass change components. The observed warming, freshening, and AOU changes in the core AAB were divided into meridional shifts and water-mass change components. The meridional shift components were estimated as a product of the meridional gradients (e.g., Fig. S4b, e) and anomalies in the meridional position of SACCF (estimated by dividing SACCF depth anomaly in Fig. S5 by mean topographic gradient in the core AAB). Then, water-mass change components of observed changes were estimated by subtracting the meridional shift components from the observed changes as follows:

$$\Delta\theta_{d,i,\text{watermass}} = \Delta\theta_{d,i} - \left. \frac{\partial\theta}{\partial y} \right|_d \Delta y_i, \quad (2)$$

where $\Delta\theta_{d,i,\text{watermass}}$ is water-mass change component for potential temperature, $\left. \frac{\partial\theta}{\partial y} \right|_d$ is meridional gradient of potential temperature, and Δy_i anomalies in the meridional position of SACCF. Water mass change components for salinity and AOU changes also follow the Eq. (2) and definitions of d and i are the same with previous subsection. Then, linear trends for water mass changes were obtained at each isobaric surface using the least-squares method for $\Delta\theta_{d,i,\text{watermass}}$ and $\Delta S_{d,i,\text{watermass}}$ as shown in Fig. 4.

Estimation of errors. In this study, multi-decadal trends and their errors were estimated in the core AAB, SAB, and the overall AAB, where data availability varies considerably. Hence, different methods were applied to these regions based on data availability.

In the core AAB, we estimated the multi-decadal trends using combined data observed at different sections, as described in previous subsections. The choice of the error estimation method is important. The mesoscale (~163 km) feature was important for estimations of the multi-decadal variability based on data obtained in the same section, which were repeated once or twice during the past few decades⁶. Multi-decadal variability, based on annually conducted observations in the core AAB, however, revealed relatively evident inter-annual variability (e.g., Figs. 3 and S5). Thus, we adopted the uncertainty of the estimated slope to estimate the confidence interval (hereafter referred to as CI) for the isobaric trends (Figs. 2b, c, 4, 5a, b, and S7g, h) and steric SLR trends (Table 1), as described in the next paragraph. For the multi-decadal trends in the SAB and overall the AAB, estimated using the WOCE/GO-SHIP section data, we followed previously described methodologies⁶ to estimate the multi-decadal trends and their errors (isobaric trends shown in Figs. 5d, e and S7a–f).

CIs of estimated trends in the core AAB were assessed assuming a Student's t distribution as follows. For linear trends in the core AAB, the uncertainty in the slope was adopted for the CI as follows:

$$\text{CI} = t_{a/2,N-1} S, \quad (3)$$

where $t_{a/2,N-1}$ is a Student's t multiplier, which depends on the significance level (a) and degrees of freedom (N), and S is the standard error of the regression coefficient. N is given by the number of sections throughout the time series (i.e., 12). For vertically averaged trends (e.g., AABW warming and freshening trends discussed in the result section), the CI estimated for each isobaric surface was vertically averaged.

For the steric SLR estimated for each section (shaded grey and black areas in Fig. 3), the standard deviations of the potential temperature and salinity changes from 1995 were estimated for each isobaric surface and converted to CIs as follows:

$$\text{CI} = t_{a/2,N-1} \frac{S}{\sqrt{N}}, \quad (4)$$

where $t_{a/2,N-1}$ is the same as that in Eq. (3), where S is the standard deviation, and N is the number of observations in each section. Then, the CIs were converted to the SLR form using Eq. (1) and vertically integrated.

Estimation of changes in the total AOU and required DSW supply. Changes in the total AOU and required change in DSW supply were estimated based on obtained AOU trends in the core AAB and along the WOCE/GO-SHIP sections. Differences in the condition of the southward shift in the ACC fronts between the AAB and SAB (Supplementary Note S5) should be taken account during this process. In the SAB, where the southward shift is not clear, the total AOU changes were simply obtained based on the AOU trends estimated from the three WOCE/GO-SHIP sections using previously described methodologies⁶ (Fig. S7b). For the AAB, however, considering the evident southward shift, water mass changes obtained in the core AAB (Fig. 5b) were extrapolated throughout the basin. Considering that the estimation is influenced by interpolation errors induced by the extrapolation of results obtained from limited region to the overall basin, we also estimated the total AOU changes using the manner same as the SAB. Having no evidence to conclude which estimate is more realistic, we adopted mean values, while the differences in these two estimates are especially large in the less dense LMOC (Table S2).

Regarding the integration interval for the SAB, climatological isopycnals of 28.02 and 28.19 kg m^{-3} were determined from data obtained along the three sections, with a previously proposed interpolation method³². The volume-weighted mean trends and errors were estimated for the densest LMOC ($\gamma^\sigma > 28.19 \text{ kg m}^{-3}$) and for the less dense LMOC ($28.02 \text{ kg m}^{-3} > \gamma^\sigma > 28.19 \text{ kg m}^{-3}$) using previously described methodologies⁶. Then, the total masses in the respective intervals were multiplied to obtain total the AOU changes and their errors. For the AAB, the volume-weighted mean trends and errors were estimated for the densest LMOC ($\gamma^\sigma > 28.32 \text{ kg m}^{-3}$) and for the less dense LMOC ($28.02 \text{ kg m}^{-3} < \gamma^\sigma < 28.19 \text{ kg m}^{-3}$) in the same manner as the SAB. We selected an isopycnal of $\gamma^\sigma = 28.32 \text{ kg m}^{-3}$ as the upper boundary of the densest LMOC in the AAB because AOU increase became evident below this layer (roughly corresponding to a depth of 3900 m; Fig. 5b).

Then, the required change in the DSW supply was estimated by adopting the typical properties observed for High Salinity Shelf Water (HSSW) in the Ross Sea (AOU: 86.2 $\mu\text{mol kg}^{-1}$, θ : -1.91°C , γ^σ : 28.74 kg m^{-3}) as follows:

$$\Delta V_{\text{trDSW}} = \frac{\Delta\text{AOU}}{(\text{AOU}_{\text{DSW}} - \text{AOU}_{\text{Basin}})\rho_{\text{DSW}}}, \quad (5)$$

where ΔV_{trDSW} is the required change in DSW supply, ΔAOU is the estimated total AOU changes in the respective layers and basins, AOU_{DSW} is AOU of DSW, $\text{AOU}_{\text{Basin}}$ is a climatological mean AOU in the respective layers and basins, and ρ_{DSW} is the density of DSW. Table S2 summarizes the estimated results for total AOU changes and required changes in DSW supply.

Data availability

Hydrographic data from WOCE/GO-SHIP sections are available online at <https://cchdo.ucsd.edu/>. Satellite altimetry and AAO index data are available through the Copernicus Marine Environment Monitoring Service (<http://www.marine.copernicus.eu>) and NOAA (http://www.cpc.ncep.noaa.gov/products/precip/CWlink/daily_ao_index/ao_index.html), respectively. Hydrographic data from Umitaka-Maru observations (section along 110° and 115°E) are available at <https://ads.nipr.ac.jp/data/meta/A20220329-001>.

Code availability

The Fortran codes and Generic Mapping Tools scripts used to analyse the data and to generate the figures are available from the corresponding author on request.

Received: 1 July 2021; Accepted: 27 April 2022;

Published online: 19 May 2022

References

- Purkey, S. G. & Johnson, G. C. Antarctic Bottom Water warming and freshening: contributions to sea level rise, ocean freshwater budgets, and global heat gain. *J. Clim.* **26**, 6105–6122 (2013).
- Rhein, M. et al. *Climate Change 2013: The Physical Science Basis. Contribution of Working Group I to the Fifth Assessment Report of the Intergovernmental*

- Panel on Climate Change* (eds Stocker, T. F. et al.) (Cambridge University Press, 2013), 255–315.
3. Jacobs, S. S. Bottom water production and its links with the thermohaline circulation. *Antarct. Sci.* **16**, 427–437 (2004).
 4. Johnson, G. C. Quantifying Antarctic bottom water and North Atlantic deep water volumes. *J. Geophys. Res.* **113**, C05027 (2008).
 5. Rye, C. D. et al. Rapid sea-level rise along the Antarctic margins in response to increased glacial discharge. *Nat. Geosci.* **7**, 732–735 (2014).
 6. Purkey, S. G. & Johnson, G. C. Warming of global abyssal and deep Southern Ocean Waters between the 1990s and 2000s: Contributions to global heat and sea level rise budgets. *J. Clim.* **23**, 6336–6351 (2010).
 7. Purkey, S. G. & Johnson, G. C. Global contraction of Antarctic Bottom Water between the 1980s and 2000s. *J. Clim.* **25**, 5830–5844 (2012).
 8. Shimada, K., Aoki, S., Ohshima, K. I. & Rintoul, S. R. Influence of Ross Sea Bottom Water changes on the warming and freshening of the Antarctic Bottom Water in the Australian–Antarctic basin. *Ocean Sci.* **8**, 419–432 (2012).
 9. van Wijk, E. M. & Rintoul, S. R. Freshening drives contraction of Antarctic Bottom Water in the Australian Antarctic Basin. *Geophys. Res. Lett.* **41**, 1657–1664 (2014).
 10. Shadwick, E. H. et al. Glacier tongue calving reduced dense water formation and enhanced carbon uptake. *Geophys. Res. Lett.* **40**, 904–909 (2013).
 11. Aoki, S., Kobayashi, R., Rintoul, S. R., Tamura, T. & Kusahara, K. Changes in water properties and flow regime on the continental shelf off the Adélie/George V Land coast, East Antarctica, after glacier tongue calving. *J. Geophys. Res.* **122**, 6227–6294 (2017).
 12. Jacobs, S. S. & Giulivi, C. F. Large multidecadal salinity trends near the Pacific–Antarctic continental margin. *J. Clim.* **23**, 4508–4524 (2010).
 13. Katsumata, K., Nakano, H. & Kumamoto, Y. Dissolved oxygen change and freshening of Antarctic Bottom water along 62°S in the Australian–Antarctic Basin between 1995/1996 and 2012/2013. *Deep Sea Res. II* **114**, 27–38 (2015).
 14. Chapman, C. C. New perspectives on frontal variability in the Southern Ocean. *J. Phys. Oceanogr.* **47**, 1151–1168 (2017).
 15. Orsi, A. H., Johnson, G. C. & Bullister, J. L. Circulation, mixing, and production of Antarctic Bottom Water. *Prog. Oceanogr.* **43**, 55–109 (1999).
 16. Aoki, S. et al. Widespread freshening in the Seasonal Ice Zone near 140°E off the Adélie Land Coast, Antarctica, from 1994 to 2012. *J. Geophys. Res. Oceans* **118**, 6046–6063 (2013).
 17. Menezes, V. V., Macdonald, A. M. & Schatzman, C. Accelerated freshening of Antarctic Bottom Water over the last decade in the Southern Indian Ocean. *Sci. Adv.* **3**, e1601426 (2017).
 18. Schodlok, M. P. & Tomczak, M. The circulation south of Australia derived from an inverse model. *Geophys. Res. Lett.* **24**, 2781–2784 (1997).
 19. Rintoul, S. R. On the origin and influence of Adélie Land Bottom Water, Ocean, Ice and Atmosphere: interactions at Antarctic Continental Margin. *Antarct. Res. Ser.* **75**, 151–171 (1998).
 20. Williams, G. D., Bindoff, N. L., Marsland, S. J. & Rintoul, S. R. Formation and export of dense shelf water from the Adélie Depression, East Antarctica. *J. Geophys. Res.* **113**, C04039 (2008).
 21. Williams, G. D. et al. Antarctic Bottom Water from the Adélie and George V Land coast, East Antarctica (140–149 E). *J. Geophys. Res.* **115**, C04027 (2010).
 22. Kitade, Y. et al. Antarctic bottom water production from the Vincennes bay polynya, east Antarctica. *Geophys. Res. Lett.* **41**, 3528–3534 (2014).
 23. Watanabe, Y. W. et al. Probability of a reduction in the formation rate of the subsurface water in the North Pacific during the 1980s and 1990s. *Geophys. Res. Lett.* **28**, 3289–3292 (2001).
 24. Meredith, M. P. & Hogg, A. M. Circumpolar response of Southern Ocean eddy activity to a change in the Southern Annular Mode. *Geophys. Res. Lett.* <https://doi.org/10.1029/2006GL026499> (2006).
 25. Screen, J. A., Gillett, N. P., Stevens, D. P., Marshall, G. J. & Roscoe, H. K. The role of eddies in the Southern Ocean temperature response to the Southern annular mode. *J. Clim.* **22**, 806–818 (2009).
 26. Orsi, A. H., Smethie, W. M. & Bullister, J. L. On the total input of Antarctic waters to the deep ocean: A preliminary estimate from chlorofluorocarbon measurements. *J. Geophys. Res.* **107**, 3122 (2002).
 27. Meredith, M. Replenishing the abyss. *Nature Geosci.* **6**, 166–167 (2013).
 28. Aoki, S. et al. Reversal of freshening trend of Antarctic Bottom Water in the Australian–Antarctic Basin during 2010s. *Sci. rep.*, 14415, 14415. *Sci. Rep.* **10**, 14415 (2020).
 29. Castagno, P. et al. Rebound of shelf water salinity in the Ross Sea. *Nat. Commun.* **10**, 5441 (2019).

30. Silvano, A. et al. Recent recovery of Antarctic Bottom Water formation in the Ross Sea driven by climate anomalies. *Nat. Geosci.* **13**, 780–786 (2020).
31. Siegenthaler, U. & Sarmiento, J. L. Atmospheric carbon dioxide and the ocean. *Nature*. **365**, 119–125 (1993). (1993).
32. Shimada, K., Aoki, S. & Ohshima, K. I. Creation of a gridded dataset for the Southern Ocean with a topographic constraint scheme. *J. Atmos. Ocean. Technol.* **34**, 511–532 (2017).
33. Rintoul, S. R. Rapid freshening of Antarctic Bottom Water formed in the Indian and Pacific Oceans. *Geophys. Res. Lett.* **34**, L06606 (2007).
34. Orsi, A. H., Whitworth, T. & Nowlin, W. D. On the meridional extent and fronts of the Antarctic Circumpolar Current. *Deep Sea Res. I* **42**, 641–673 (1995).

Acknowledgements

We would like to express our heartfelt appreciation to all members of the Japanese Antarctic Research Expedition (JARE) Program 52–60th for their support. We would also like to thank all officers, crew members, and researchers who contributed to the hydrographic observations and water sampling on Umitaka-Maru. We are deeply grateful to Drs. Shintaro Takao, and Masato Moteki for their indispensable contribution to the CTD observations for the JARE research project. We also thank Dr. Takeshi Terui for helping us to increase the efficiency of the observations by providing weather forecast data during the cruises. This work was supported by MEXT for physical and chemical oceanographic observations as part of the JARE (Program Grant Number JPMXD1200000000), and by JSPS KAKENHI (Grant Number JP15H01726, JP21H04918, and JP21H03587).

Author contributions

K.S. conceived the study with contributions from Y.K., S.A., K.M., and L.C.; K.S., Y.K., S.A., K.M., L.C., K.T., and R.M. conducted the Umitaka-Maru observations; K.S. performed raw data processing and subsequent quality control for the CTD data; J.K. and T.O. secured funding for the research and contributed to observation planning. All authors discussed the results and contributed to the final version of the manuscript.

Competing interests

The authors declare no competing interests.

Additional information

Supplementary information The online version contains supplementary material available at <https://doi.org/10.1038/s43247-022-00445-2>.

Correspondence and requests for materials should be addressed to Keishi Shimada.

Peer review information *Communications Earth & Environment* thanks the anonymous reviewers for their contribution to the peer review of this work. Primary Handling Editors: Regina Rodrigues, Heike Langenberg. Peer reviewer reports are available.

Reprints and permission information is available at <http://www.nature.com/reprints>

Publisher's note Springer Nature remains neutral with regard to jurisdictional claims in published maps and institutional affiliations.



Open Access This article is licensed under a Creative Commons

Attribution 4.0 International License, which permits use, sharing, adaptation, distribution and reproduction in any medium or format, as long as you give appropriate credit to the original author(s) and the source, provide a link to the Creative Commons license, and indicate if changes were made. The images or other third party material in this article are included in the article's Creative Commons license, unless indicated otherwise in a credit line to the material. If material is not included in the article's Creative Commons license and your intended use is not permitted by statutory regulation or exceeds the permitted use, you will need to obtain permission directly from the copyright holder. To view a copy of this license, visit <http://creativecommons.org/licenses/by/4.0/>.

© The Author(s) 2022